NJC

Problems With Solutions: Manipulating Alkylammonium Additive Reactivity for Durable High-Quality Perovskite Films

Journal:	*New Journal of Chemistry*
Manuscript ID	NJ-ART-09-2024-003915.R2
Article Type:	Paper
Date Submitted by the Author:	10-Dec-2024
Complete List of Authors:	Palmer, Jack; University of California San Diego, Chemical and Nano Engineering Iwamoto, Soichiro; UC San Diego Han, Clark; University of California San Diego, Nanoengineering Dolan, Connor; University of California San Diego, Nanoengineering Vossler, Hendrik ; University of California San Diego, NanoEngineering Dunfield, Sean; University of California San Diego, Nanoengineering Fenning, David; University of California San Diego, NanoEngineering

ARTICLE

Problems With Solutions: Manipulating Alkylammonium Additive Reactivity for Durable High-Quality Perovskite Films

Received 00th January 20xx,
Accepted 00th January 20xx

DOI: 10.1039/x0xx00000x

Jack R. Palmer[a], Soichiro Iwamoto[b], Clark Han[b], Connor J. Dolan[b], Hendrik M. Vossler[a], Sean P. Dunfield[b]*, David P. Fenning[a,b]*

Methylammonium chloride (MACl) is used as a volatile additive in many high-efficiency formamidinium lead iodide ($FAPbI_3$) perovskite solar cells. However, MA is known to irreversibly react with FA to form n-methyl formamidinium (nMFA), which is detrimental to absorber quality. In this work, we explore a series of alternative alkylammonium chlorides (RACls) in an antisolvent-free deposition. We analyze their reactivity toward FA in precursor inks and their effect on perovskite thin film crystallinity, photoluminescence quantum yield (PLQY), and durability under light and heat. We find that the length and branching of the alkyl chain has a significant effect on reaction rate with FA, with isopropylammonium (iPA) showing a 10 times slower reaction rate than MA. For films cast with the RACl additives, diffraction intensity of the (001) perovskite peak is maximized with ethylammonium (EA) and iPA, then decreases with further increases in alkyl chain length. Full width at half maximum of the (001) perovskite diffraction peak is smaller for all additives relative to the MACl control, with iPA maintaining a low FWHM after a week of precursor solution aging. Importantly, films cast from solutions aged for one week containing the alternative RACl additives all formed black perovskite α-phase, while the MACl controls did not, highlighting the negative impact of nMFA. PLQY of films made with alternative additives both before and after solution aging is comparable to pristine MACl. Durability tests of unencapsulated films in inert atmosphere under white light and 85˚C heating revealed increased stability of the black perovskite α-phase by replacing MA, with iPA and nBA offering the best phase stability. The results presented herein demonstrate promising alternative volatile additives to replace MACl in $FAPbI_3$-based perovskite solar cells.

1 Introduction

Perovskite solar cells (PSCs) have achieved high efficiencies relative to their detailed balance limits in recent years, reaching >80% of the theoretical limit.(1) Many record-setting devices have converged toward an absorber layer composed of mainly formamidinium lead triiodide ($FAPbI_3$) with methylammonium chloride (MACl) as an additive in solution.(2,3) MACl serves several functions as an additive, including increasing apparent crystalline domain size, forming a crystalline intermediate, and leaving residual MA in the lattice to relax the tolerance factor, “stabilizing” the initial cubic perovskite crystal structure.(2) Chemically, MACl is the hydrochloride salt of methylamine, a primary amine. Because MA is a weak acid, there exists an equilibrium in solution between MA and the free amine, methylamine (MA^0), which is described by the pKa of MA in that solution. Methylamine is an important synthetic building block, owing mainly to its high nucleophilicity enabling facile molecular functionalization.(4) Although MA is commonly used as an A-site in perovskite solar cells (PSCs), there is evidence that its relatively low pKa and the high nucleophilicity of methylamine make it an unsuitable candidate for commercial photovoltaics.(5)

Solution chemistry, including chemical reactions in inks, is known to strongly influence the final perovskite film.(6,7) Of particular importance is the reaction between MA and FA: $MA^0 + FA^+ \rightarrow nMFA^+ + NH_3$, which has been shown to occur in the liquid phase(8), during annealing,(9) and to a limited extent, in the solid state film.(10) This reaction irreversibly produces n-methyl formamidinium (nMFA), which severely damages optoelectronic quality and even completely inhibits black perovskite phase formation at relatively low concentrations.(11) This reaction also produces ammonia, which can either leave the film or solubilize the perovskite, leaving voids in the film.(12) There are two major steps required for this reaction to go forward: 1) deprotonation of the MA cation to form methylamine: $MA^+ \rightarrow MA^0 + H^+$ and 2) nucleophilic attack by methylamine on FA: $MA^0 + FA^+ \rightarrow nMFA^+ + NH_3$. By recognizing these distinct reaction steps, alternative additives to MA may be rationally designed to minimize the formation of deleterious side products.

To target the first step in the reaction, deprotonation, various high-pKa additives, such as guanidinium (Gua^+), have been reported in the literature.(13–15) For example, De Marco et al. reported the use of Gua^+ as an additive in perovskite solar

[a] Materials Science and Engineering Program, University of California, San Diego, La Jolla, California 92093, USA.
[b] Department of Chemical and Nano Engineering, University of California, San Diego, La Jolla, California 92093, USA
Supplementary Information available: [details of any supplementary information available should be included here]. See DOI: 10.1039/x0xx00000x

cells and observed enhanced carrier lifetimes and device performance.(15) Recent works have successfully employed Gua^+ as a surface treatment. For example, Chen et al.(13) demonstrated increased device durability and performance upon treatment with Gua. The spontaneous reaction of a free amine with an FA cation also generalizes to other common chemicals used in perovskite processing. For example, Jiang et al.(16) use the reaction of a free amine (3-(aminomethyl)pyridine) with FA to their advantage in a post-treatment of a $FAPbI_3$ perovskite layer to simultaneously achieve *n*-type doping and passivation of the film surface, leading to enhanced stability and efficiency of a *p-i-n* device. In another work, Wang et al.(12) report that phenethylammonium (PEA^+), a common 2D forming additive, contributed significantly to device degradation under light and heat due to the relatively low pKa of its ammonium group, causing deprotonation and subsequent reaction with FA to form (phenethylamino)methaniminium ($PEAMA^+$). The authors avoid this degradation pathway by using the high pKa reaction product ($PEAMA^+$) itself as a surface treatment to suppress deprotonation, resulting in much improved device stability.

A key consideration in the subsequent, nucleophilic attack step is the steric bulk of the amine. Methylamine is a relatively small molecule with low steric hinderance, resulting in a facile reaction with FA. Various alkylammonium chlorides larger than MACl have been reported in the literature. Ethylammonium, at just one methylene group larger than MA, has been demonstrated as an additive(17–22) and as an A-site cation in the perovskite lattice.(23,24) N-propylammonium, iso-propylammonium, and n-butylammonium have also been reported as additives(3,25) and as surface treatments,(26) enabling promising performance owing to surface passivation and some 2D phase formation. However, the recent work by Wang et al.(12) critically highlights the importance of additive reactivity, and generally shows that alkylammonium reactivity toward FA is detrimental to device operational stability. While alkylammoniums larger than MA have been effective in promoting the performance of PSCs, neither their reaction rates toward FA nor the influence of their reaction products on film properties have been reported.

In this work, we study a series of alkylammonium chlorides (ammonium, ethylammonium, n-propylammonium, isopropylammonium, and butylammonium: NH_4, EA, nPA, iPA, and nBA respectively) and evaluate their: 1) reaction rate with FA in inks, 2) ability to form quality perovskite films, and 3) perovskite phase durability under light and heat as compared with an MACl additive control. By choosing this series of increasing alkyl chain length, we sought to isolate the effect of additive size on reactivity, film optoelectronic quality, and durability. It is observed that the reaction products of all additives harm film quality less than nMFA, implying that MA is a uniquely detrimental option among the studied set of alkylammonium chloride additives. We find that iPACl displays the best combination of lowered reaction rate (factor of 10), high crystallinity, and high durability under light and heat. We attribute the effectiveness of iPACl to its steric bulk, which lowers its nucleophilicity and decreases reaction rate with FA.

2 Experimental

2.1 Materials

The following chemicals were used as received without further modification: isopropanol (HPLC grade), acetone (HPLC grade), Hellmanex III, 2-methoxyethanol (99.8%, anhydrous), 1-methyl-2-pyrrolidone (99.5%, anhydrous), ammonium chloride (99.998% trace metals basis), (3-aminopropyl)triethoxysilane (99%), and ethanol (200 proof, anhydrous) were purchased from Sigma Aldrich. PbI_2 (99.99% trace metals basis), isopropylammonium chloride (98.0+%), n-propylammonium chloride (98+%), n-butylammonium chloride (98+%), and MeO-2PACz (98+%) were purchased from TCI America. Formamidinium iodide, ethylammonium chloride, and methylammonium chloride were purchased from Greatcell. Methyl sulfoxide-d6 (99.9% atom D, for NMR) was purchased from Fisher Scientific. Microscope slides were purchased from VWR (#48300-026) and cleaved into 3 even pieces to make 1 inch square substrates.

2.2 Solution and Film Preparation

All substrates were treated with the following procedure before deposition: 15 minute sonication each in 2% Hellmanex-III/DI H_2O, DI H_2O, acetone, and IPA followed by a 20 minute UV-Ozone treatment. To prepare the perovskite precursor solution, PbI_2 (1.33 mmol), FAI (1.33 mmol) were dissolved in 1mL of 2-methoxyethanol (2-ME) and vortexed for 1 hour. To a vial containing the RACl salt at the desired concentration, 1mL of $FAPbI_3$ solution was added and vortexed for <5 min until completely dissolved. Finally, 7.5% by volume of NMP (75 µL) was added and gently vortexed for 1 min. The solution was used within one hour to minimize unwanted reaction products unless otherwise indicated. To age the solutions, the vials were capped tightly, sealed with parafilm, and kept in an N_2 glovebox until further use.

All glass substrates were spincoated with 100µL of 0.6 mg/mL MeO-2PACz in EtOH at 3000 rpm for 30 s, then annealed at 100°C inside a N_2 glovebox. Glass substrates were coated with MeO-2PACz to mildly passivate the float glass surface, enabling more repeatable photoluminescence results. Once the substrates were cooled, 100µL of perovskite precursor solution was deposited onto the substrate and spin coated for 30 seconds at 8000 rpm with a ramp rate of 2000 rpm/s, then annealed at 150°C for 10 minutes. Samples used for photoluminescence were treated with (3-aminopropyl)triethoxysilane (APTES) following the procedure of Jariwala et al.(27)

2.3 Proton Nuclear Magnetic Resonance

Inside of a N_2-filled glovebox (<1ppm O_2, H_2O), 0.5M of $FAPbI_3$ and 0.075M RACl were dissolved in deuterated DMSO (DMSO-d6, Sigma Aldrich, 99.9%) and vortexed for several hours to fully dissolve. The samples were transferred into glass NMR tubes (NORELL) using clean single use glass pipettes. Pure DMSO-d6 was measured as a control for all NMR measurements. All NMR tubes were filled to a solution height

of 4 cm and sealed with a cap and tightly parafilmed before removal from the glovebox. ^{1}H-NMR measurements were carried out using a Jeol ECZ 400MHz NMR Spectrometer at room temperature. 64 scans were measured and averaged for each sample with an acquisition time of 2 seconds and a relaxation time of 4 seconds, employing force tune. The pure DMSO-d6 was analyzed first to ensure the absence of contaminants in the solvent. The NMR data was processed using MestReNova software. The central peak of DMSO was calibrated to 2.5 ppm.

2.4 Material Characterization

X-ray diffraction measurements were carried out using an Anton Paar XRDynamic 500 in Bragg-Brentano beam geometry, and coupled scans were taken from 3°-45° 2θ. Cu-K_α radiation was used with a tube voltage of 40kV at 50mA of current. Scans were collected in continuous mode with a step size of 0.005˚ for a total scan time of 11.5 minutes. Scanning electron micrographs were collected in secondary electron imaging mode using in-lens detection on an FEI Apreo SEM, with beam energy and current fixed at 2kV and 50pA respectively. Samples were imaged on glass substrates with no further preparation. No significant charging was observed. Attenuated total reflectance Fourier transform infrared spectroscopy (ATR-FTIR) was collected using a Perkin Elmer Spectrum Two with a diamond window. Prior to measuring samples, the diamond window was wiped with isopropanol and a background scan was collected. FTIR data was collected at a resolution of 0.5 cm^{-1} averaged over 32 scans. Camera images of films were corrected for brightness and contrast using an internal standard image.

2.5 Degradation under Illumination and Heating

Degradation experiments were carried out using a custom setup consisting of a sealed aluminum box held at ~2psi N_2 overpressure to keep the samples under inert atmosphere. Through a quartz window on the box, samples were illuminated with ~0.6 suns equivalent photon flux (Viparspectra XS4000, spectrum in Figure S25) and held at 85°C using a custom-built aluminum hotplate under PID control. Data was collected in the form of RGB images using a silicon CMOS camera (GoPro). The intensity of the red pixel channel across each sample area was averaged and plotted against time to quantify degradation, as the primary signal was the transition of black photoactive perovskite phase to inactive yellow phase.

2.6 Photoluminescence Quantum Yield and Implied Current-Voltage Curves

Implied current-voltage (*iJV*) curves of passivated perovskite films were calculated from injection-dependent photoluminescence quantum yield (PLQY) measurements as previously reported.(28) PLQY measurements were performed on each sample using a home-built setup consisting of an integrating sphere (Newport, Model 819C-SF-4) and using the three-measurement approach.(29) Samples were excited with a continuous wave diode pumped solid state 532nm laser controlled by a laser diode controller (SRS, Model LD502). One port of the integrating sphere was fitted with a switchable-gain Si photodetector (Thorlabs, PDA100A2) with an automated filter slider (Thorlabs, ELLK6) loaded with a 600nm longpass filter (Thorlabs, FELH600, O.D. 6). The laser was modulated at 993Hz and photodetector signal was read using a lock-in amplifier (SRS, SR830). To determine the implied voltage (*iV*) values across the range of illumination conditions, the following formula was used:

$$iV = V_{lim}(J_{ill}) + \frac{k_B T}{q} ln(PLQY)$$

where k_B is the Boltzmann constant, T is the absolute temperature of the sample (fixed at 300K), q is the elementary charge, and $V_{lim}(J_{ill})$ is the radiative voltage limit as a function of photocurrent. Implied voltage is directly proportional to the quasi-Fermi level splitting (QFLS), a parameter limited by non-radiative recombination, which is quantified through PLQY. The implied current density values were scaled down to 90% to represent 10% loss of photocurrent due to optical losses.

3 Results and Discussion

3.1 Solution Reactivity

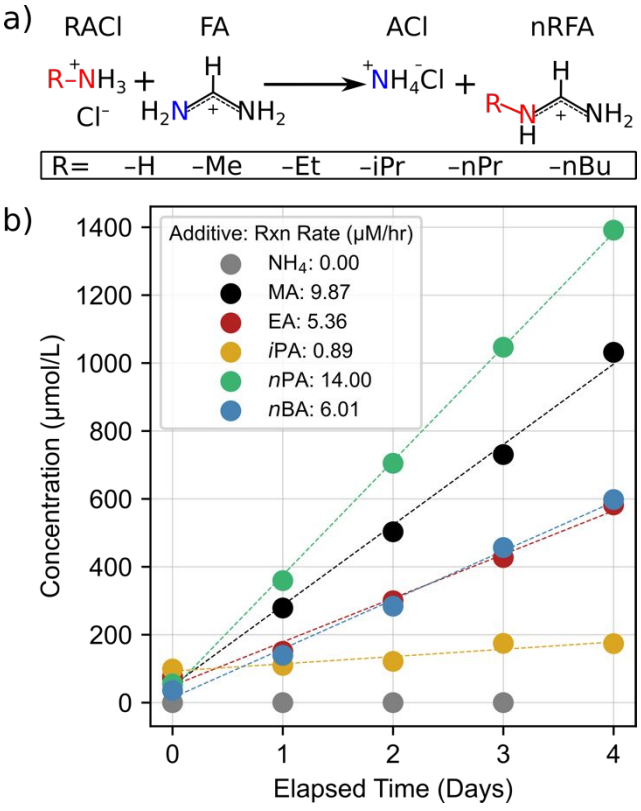

Figure 1: (a) General reaction scheme for RACl with FA^+. (b) Quantified NMR of the reaction product over 5 days.

First, we sought to understand the reaction rates of formamidinium (FA) with NH_4Cl, MACl, EACl, iPACl, nPACl, and

nBACl in solution. Molecular structures of all additive cations are shown in Figure S1. To study reaction rate, ^{1}H NMR spectra of solutions containing $FAPbI_3$ and the RACl in DMSO-d6 were collected daily over a period of 5 days. Distinct products evolved via the generalized reaction scheme in Figure 1a were identified for each RACl and quantified (details in Supplementary Note 1). We note that NH_4Cl was included as a control condition for RACl reactivity, since the product of the reaction between NH_4^+ and FA^+ simply reforms NH_4^+. Reaction product concentrations are shown as a function of time in Figure 1b, with the slope of linear fits representing the reaction rate. Most notably, the reaction rate of iPA (0.89 μM*hr^{-1}) is lower than MA (9.87 μM*hr^{-1}) by a factor of ~10, while its structural isomer nPA (14.0 μM*hr^{-1}) has a reaction rate that is slightly higher than MA. Considering that the pKa of iPA and nPA are similar, this difference in reactivity is most likely due to the increased steric bulk of iPA increasing the activation energy of nucleophilic attack on the FA cation. EA and nBA display similar reaction rates of 5.36 μM*hr^{-1} and 6.01 μM*hr^{-1} respectively, which is significantly lower than MA (9.87 μM*hr^{-1}). The reaction rates of EA and nBA are possibly slowed due to the increased chain length relative to MA; however, this trend in reaction rate is broken with nPA, which displayed the highest reaction rate. We will not speculate on the cause of the increased reactivity of nPA but note that it was reproducible. Moving on from solution reactivity, we turn to focus on the effect of each RACl and its reaction product on the formation of $FAPbI_3$ thin-films.

3.2 X-ray Diffraction

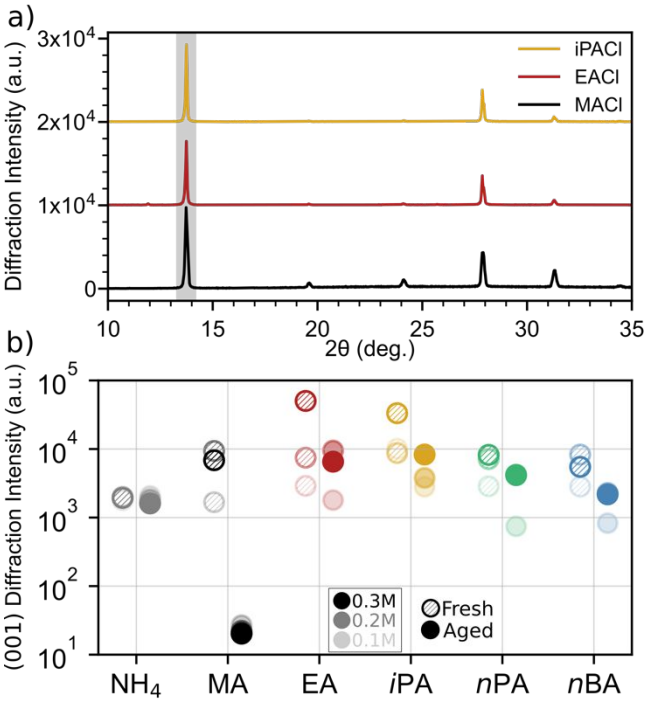

Figure 2: (a) Diffraction patterns for $FAPbI_3$ films cast from fresh inks with 0.2M MACl (control) and 0.2M EACl and iPACl additives. (b) Fitted (001) 3C-$FAPbI_3$ (α-phase) diffraction intensity for films cast from fresh and aged inks. Increasing opacity represents increasing RACl concentration (0.1, 0.2, and 0.3M).

X-ray diffraction intensity of $FAPbI_3$ films produced with RACl additives are presented in Figure 2. To highlight the potential of films produced with EACl and iPACl to achieve parity with MACl films, Figure 2a shows diffraction patterns for $FAPbI_3$ films cast from fresh inks with 0.2M MACl (control), 0.2M EACl, and 0.2M iPACl additives. All conditions are shown in Figure 2b on a semi-log plot, where only the intensity of fitted (001) 3C-$FAPbI_3$ (α-phase) peak is shown to facilitate comparisons, with full XRD patterns in Figures S2-S9. EA and iPA produce highly crystalline (001)-oriented films, reaching a maximum diffraction intensity and orientation at 0.3M RACl, and retain a significant portion of that crystallinity in films formed after aging the ink (Figure 2b). This retention of crystalline quality is in stark contrast to MA, where no 3C-$FAPbI_3$ was detected in films cast from aged solutions. MA was the only additive that did not retain any α-phase in films cast after solution aging. The negative impact of nMFA on perovskite film formation is well documented in the literature(6,7); however, Figure 2b highlights the uniquely harmful nature of nMFA in the context of other chemically similar additives.

With increasing alkyl chain length in nPA and nBA, decreasingly crystalline films are produced, possibly due to the size of the additive disrupting crystallization and even forming some lower-dimensional phases (Figures S7 and S9). Specifically, nPA and nBA which are commonly used 2D forming additives, show low dimensional diffraction peaks around 8˚ 2θ in the films cast from fresh inks, which increase in intensity in the films made from aged inks. We attribute this bias toward formation of low-dimensional phases after aging to the vapor pressure of the alkylammonium conjugate base and size of the reaction product. In the freshly prepared solution, the ammonium group is deprotonated, allowing the alkylamine and HCl to leave the film, following this reaction: RA^+Cl^- + Heat → RA^0 + HCl. During ink aging, the $RAFA^+$ reaction product is formed, which has a much higher pKa(12) and does not leave the film during the anneal.

This argument that the amine-FA reaction product is less volatile is supported by ATR-FTIR spectra of films shown in Figure S10 and S11. Figure S10 shows FTIR absorbance in the alkyl C-H stretching region (~3100-2700 cm^{-1}), where little signal is observed in the films made from fresh inks. Upon aging, new vibrational modes unique to the longer-chained EA, iPA, nPA, and nBA are observed, which increase in intensity with increasing additive concentration. From NMR, we have identified the formation of significant amounts of $RAFA^+$ reaction product during ink aging, so we attribute these vibrational modes in FTIR to the presence of this reaction product. To further confirm the assignment to $RAFA^+$ in the films produced from aged inks, Figure S11 shows FTIR spectra in the alkyl C-H bending region (~1600-1400 cm^{-1}). Here, the same trend is observed: films cast from fresh inks display few unique peaks, while spectra of films cast from aged inks contain C-H bending modes unique to each additive, which increase in intensity with increasing additive concentration. The outlier in

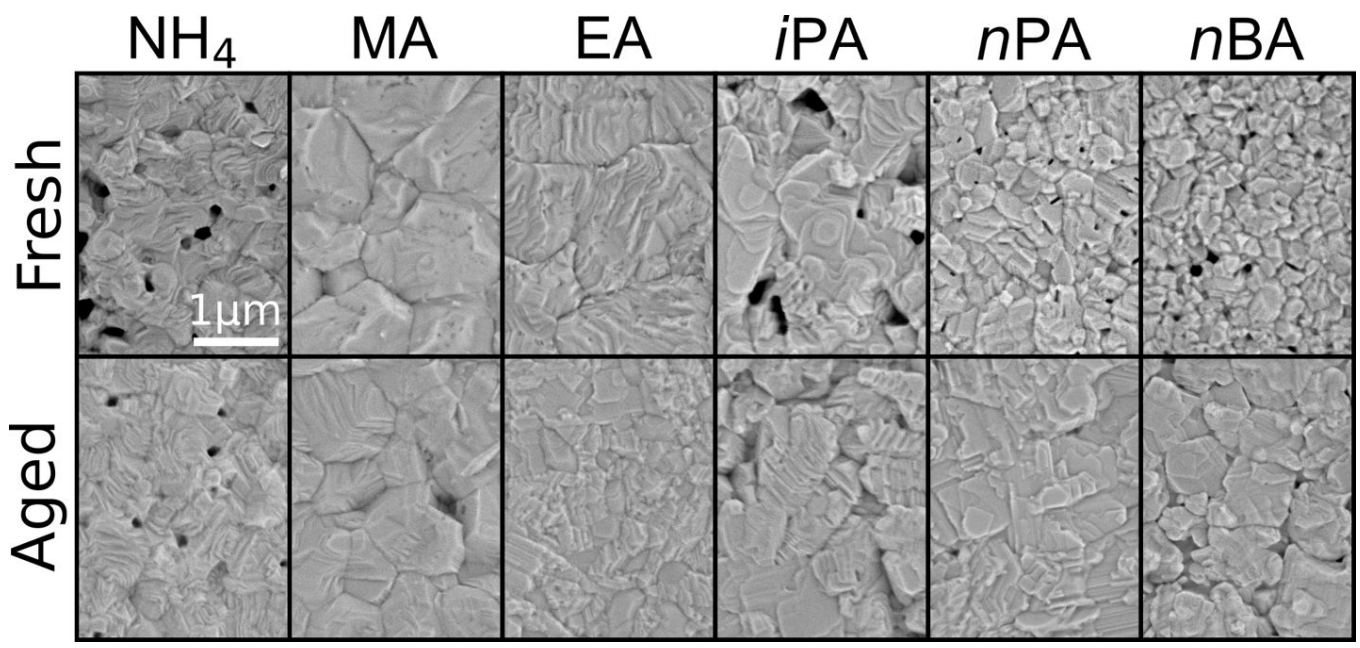

Figure 3: SEM of films cast from fresh and aged solutions prepared with 0.2M of RACl additive. The 1 μm scale bar is common to all images.

this set of data is EA, which shows a unique bending mode growing in around 1460 cm^{-1} in the films cast from fresh inks. We attribute this to the size of the EA cation, which is on the cusp of ionic radius for fitting in the perovskite lattice,(30) allowing for partial incorporation into the perovskite lattice. This is corroborated by the XRD peak growing in intensity with increasing additive concentration at ~12˚ 2θ in Figure S6c, which is likely due to partial formation of some $EAPbI_3$ phase in the film.(23)

In the films made from fresh inks, the full width at half maximum (FWHM) of the (001) perovskite diffraction peak is generally lowered with increasing additive concentration, likely indicating greater uniformity of *d*-spacing within the film (Figure S12). A minimum FWHM of 0.065˚ 2θ achieved by 0.3M EACl. Films produced from fresh inks with MACl have a FWHM slightly higher than other additives, potentially due to MA incorporating into the lattice, producing a broader distribution of *d*-spacing. Upon ink aging, iPACl films retained their low FWHM; EA, nPA, and nBA show an increase in FWHM, and MACl films did not form α-phase perovskite during annealing. We attribute this to the lowered reactivity of iPA, resulting in less reaction product in the film made from aged precursors, thus retaining its narrowed distribution of *d*-spacing. To assess the microstrain present in films, Williamson-Hall analysis was performed on the full diffraction patterns (Figure S13, S14, and Table S1). Although the films are textured, a qualitative indication of relative trends in microstrain is evident across the families of reflections that do appear in the diffraction pattern. Similar trends are observed: fresh iPA and EA films show the lowest microstrain, decreasing with increasing additive concentration, and upon ink aging iPA retains its low microstrain. For longer chain additives nPA and nBA, the microstrain is slightly higher. These results highlight the benefits of the lowered reactivity of iPA toward producing highly-crystalline perovskite thin films and the promising performance of EA.

Analysis of the low-angle diffraction intensity (5˚-12˚ 2θ) reveals increasing low-dimensional phase formation with increasing alkyl chain length. Due to the difficulty of indexing the many diffraction peaks present in some films formed from aged precursors arising due to low-dimensional phases, the diffraction patterns were integrated from 5˚-12˚ 2θ to gain qualitative insight into the presence of low-dimensional phases present in the film (Figure S15). In the films made from fresh solutions, no low-dimensional phases were formed in NH_4, MA, EA or iPA, while nPA and nBA show a minor amount of low-dimensional phase formation. Upon ink aging, all additives except for NH_4 result in an appreciable amount of low-dimensional diffraction intensity, especially in 0.3M EACl and nBACl, where the low-dimensional diffraction is dominant. These results are consistent with the ATR-FTIR spectra (Figures S10 and S11), which show more alkyl species present in the films cast from aged inks.

3.3 Film Morphology

Overall, all additives at all concentrations produced black films when cast from fresh inks (film photographs in Figures S16-S18). Among the films cast from aged inks, all additives except MACl retained their ability to form black films. To understand the microscopic morphological effect of each additive and its reaction product, scanning electron microscopy (SEM) images of films cast from fresh and aged inks prepared with 0.2M of RACl additive are presented in Figure 3, with SEM images of 0.1M and 0.3M shown in Figures S19 and S20 respectively. Beginning with NH_4Cl, the films lack distinct domains and display an appreciable pinhole density. Importantly, the morphology is unchanged with ink aging, which serves as a control to help isolate the effect of aging associated with each additive rather than other species in the ink (e.g. PbI_2, 2-ME, NMP), as NH_4 does not produce a unique reaction product with FA. MACl produced films from fresh inks

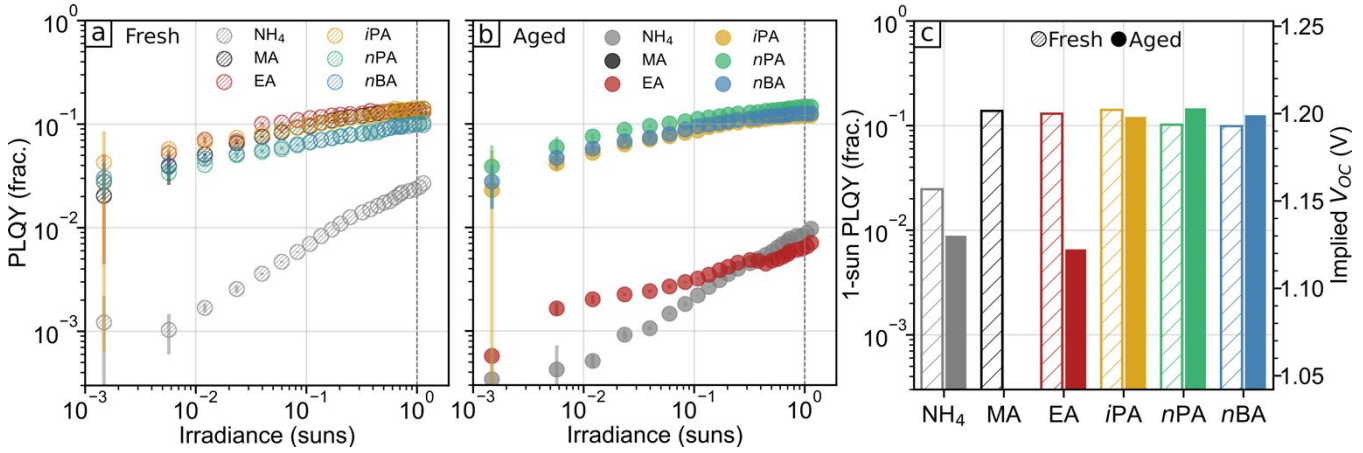

Figure 4: Implied JV curves derived from PLQY measurements of films prepared with 0.2M of the additive cast from (a) fresh and (b) aged inks. Films were passivated with APTES to limit the effect of surface recombination. (c) Bar chart of implied efficiencies under AM-1.5G illumination.

with apparent domains >1µm, while aging the ink produced films with slightly smaller grains and pinholes. EACl produced the most favorable films from fresh solutions, with large >1µm domains, low pinhole density, and a terraced surface, indicating good crystallization.(16) Upon ink aging, EACl films retain some surface terracing and low pinhole density, making it a promising candidate to replace MACl as an additive to aid film formation. iPACl yielded films from fresh inks with a terraced morphology and large apparent grain domains, yet also displayed a high pinhole density. Upon aging the ink, iPACl films retained their terraced morphology, but saw a reduction in pinhole density. We speculate that small amounts of the $RAFA^+$ reaction product may help to induce nucleation during film formation, similar to the effect of pentamindinium observed by Shi et al.(31) Fresh inks with nPACl and nBACl yielded similar film morphologies, with relatively small apparent grain domains (<300nm) and moderate pinhole densities. Interestingly, upon aging the ink, film morphology was improved, showing larger apparent domains and fewer pinholes. We again speculate that this improvement in morphology is due to the reaction product with FA aiding in film nucleation. To isolate the RACl additive as the independent variable in this work, identical film processing conditions were used across all samples facilitated by the avoidance of an anti-solvent in the deposition process through the self-volatilizing, 2-ME/NMP based ink (Experimental Methods) with a long lived intermediate and high reproducibility. While films produced with NH_4, iPA, nPA, and nBA have varying pinhole densities, methods exist in the literature, such as modifying the anneal temperature and duration, to suppress pinhole formation without significantly changing the solvent chemistry. Thus, with process engineering outside the scope of this manuscript, it is likely that pinhole-free morphologies relevant to ultimate device applications could be achieved.

3.4 Photoluminescence and Implied J-V Curves

To assess the optoelectronic quality of the $FAPbI_3$ films, injection dependent photoluminescence quantum yield (PLQY) was measured. Because the PLQY is directly related to the ratio of radiative to total recombination rates, the quasi-fermi level splitting (QFLS) can be calculated. By calculating the QFLS from PLQY data over a series of light intensities and using the bandgap extracted from PL spectra (Figures S21 and S22) an *implied* current-voltage (*iJV*) curve can be plotted to reveal the theoretical efficiency limit of a given absorber sample. In these measurements, evaluation of *bulk* flim quality was facilitated by bottom and top surface passivation by MeO-2PACz(32) and APTES(27), respectively.

Intensity-dependent PLQY of films cast from fresh and aged inks with 0.2M of RACl are shown in Figure 4a and b respectively, with 1-sun PLQY values extracted and displayed in Figure 4c. For films cast from fresh inks, all additives except NH_4 produce films with a 1-sun PLQY of >10%, which translates to an implied V_{OC} loss of <59mV from the radiative limit. When the solutions are aged and reaction products with FA are formed, films made with MACl lose all detectable photoluminescence intensity due to no formation of black α-phase perovskite. Interestingly, aging solutions containing additives with longer alkyl chains (nPA and nBA) showed slightly increased PLQY, possibly due to presence of low-dimensional phases acting to passivate grain boundaries within the film. EA decreases in PLQY after aging, possibly owing to its ability to partially incorporate in the perovskite lattice,(30) which may contribute to more crystal defects once aged, lowering PLQY. Overall, these data show that the efficiency potential for all RACl additives is on par with MACl, and the reaction products of larger RACl additives are less harmful to the optoelectronic quality compared with MA. These data are further transformed to *iJV* curves, shown in Figure S23. From these curves, an implied power conversion efficiency (*iPCE*) is calculated, representing the maximum theoretical efficiency of a solar cell made using each absorber with lossless contacts under terrestrial illumination. The trends in *iPCE* are similar to those observed in iV_{OC}, where the longer-chain additives retain their efficiency limit after aging, with iPA, nPA, and nBA all maintaining an *iPCE* >26% after aging the solution. It is also likely, given the similar PLQY and *iPCE* seen amongst the alternate RACls that the surface passivation is limiting measured radiative emission and, thus, that the PLQY

and *iPCE* may be lower bounds to film optoelectronic performance.

3.5 Light and Heat Stability

It is well-known that photoactive 3C-$FAPbI_3$ (α-phase) is thermodynamically unstable at room temperature(33) and spontaneously transforms to the more stable photoinactive 2H-$FAPbI_3$ (δ-phase). In addition to promoting grain growth during annealing, MACl also stabilizes the α-phase at room temperature via partial incorporation of MA into the lattice. While beneficial for phase stabilization, the volatility and reactivity of MA is detrimental for stability toward light and heat stressors.(10) To assess the durability of films produced with alternative RACl additives, accelerated stress testing was conducted on films produced from fresh solutions.

The color change of films after 650 hours of light and heat stress testing are presented in Figure 5, where the color varies from black to yellow from the top to bottom of the figure. MA films are seen to most completely phase-transform to the photoinactive δ-phase, while iPA and nBA are quite stable. Notably, the trends in Figure 5 roughly follow trends in solution reactivity, except for nBA, which may be more durable toward light and heat due to the longer alkyl chains decorating the surface of the grains, effectively lowering the rate of volatilization of A-site. Because the reaction of MA and FA has been shown to occur in the solid state(10,12), we speculate that the solution reactivity in Figure 5 may serve as a rough proxy for the stability observed under light and heat, where more reactive species will result in films with lower durability.(12) We note that device-level durability is a complex function of not only the bulk durability but also the interfaces with charge transport materials. Nevertheless, the significant difference in the rate of phase change in this light and heat test indicates that alternative RACls to MA hold promise for improved durability of perovskite active layers.

Conclusions

A series of alternative primary alkylammonium chloride additives (RACls) are systematically tested for their reactivity toward FA in solution, ability to form a high-quality perovskite absorber, and for perovskite film durability. Overall, most alternative RACls mitigated the disastrous effect of solution aging seen with MACl and formed high-quality perovskite films with promising implied efficiencies (*iPCE* >26%, PLQY >10%). Insights into the reaction rates and products of alkylammoniums with FA suggest that molecular design rules, such as steric bulk, can greatly improve the ink stability while retaining performance in key metrics of absorber quality. Durability of unencapsulated films under 0.6 suns and 85˚C in a N_2 atmosphere was observed to be significantly increased in all cases relative to MACl. iPACl proved to be the most promising candidate, likely due to the steric bulk of the isopropyl group reducing its rate of nucleophilic attack of FA.

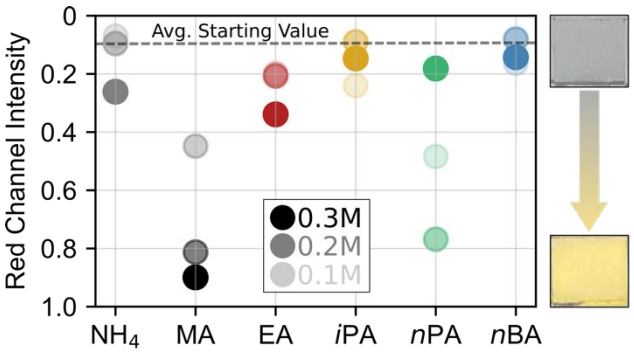

Figure 5: Film degradation data after 650 hours at 0.6 suns and 85°C in N_2 atmosphere.

Conflicts of interest

There are no conflicts to declare.

Data availability

Data is available upon reasonable request.

Acknowledgements

This work was supported in part by First Solar Inc. and by the U.S. Department of Energy, Office of Science, Office of Basic Energy Sciences under Award Number DE-SC-0023484.

References

1. Yoo JJ, Seo G, Chua MR, Park TG, Lu Y, Rotermund F, et al. Efficient perovskite solar cells via improved carrier management. Nature. 2021 Feb;590(7847):587–93.

2. Kim M, Kim GH, Lee TK, Choi IW, Choi HW, Jo Y, et al. Methylammonium Chloride Induces Intermediate Phase Stabilization for Efficient Perovskite Solar Cells. Joule. 2019 Sep 18;3(9):2179–92.

3. Park J, Kim J, Yun HS, Paik MJ, Noh E, Mun HJ, et al. Controlled growth of perovskite layers with volatile alkylammonium chlorides. Nature. 2023 Apr;616(7958):724–30.

4. Corbin DR, Schwarz S, Sonnichsen GC. Methylamines synthesis: A review. Catal Today. 1997 Aug 1;37(2):71–102.

5. Juarez-Perez EJ, Ono LK, Uriarte I, Cocinero EJ, Qi Y. Degradation Mechanism and Relative Stability of Methylammonium Halide Based Perovskites Analyzed on the Basis of Acid–Base Theory. ACS Appl Mater Interfaces. 2019 Apr 3;11(13):12586–93.

6. Chen L, Hu M, Lee S, Kim J, Zhao ZY, Han SP, et al. Deciphering Reaction Products in Formamidine-Based Perovskites with Methylammonium Chloride Additive. J Am Chem Soc. 2023 Dec 20;145(50):27900–10.

7. Dong Q, Shang W, Yu X, Yin Y, Jiang C, Feng Y, et al. Critical Role of Organoamines in the Irreversible Degradation of a Metal Halide Perovskite Precursor Colloid: Mechanism and Inhibiting Strategy. ACS Energy Lett. 2022 Jan 14;7(1):481–9.

8. Wang X, Fan Y, Wang L, Chen C, Li Z, Liu R, et al. Perovskite Solution Aging: What Happened and How to Inhibit? Chem. 2020 Jun 11;6(6):1369–78.

9. Liu R, Li Z, Chen C, Rao Y, Sun X, Wang L, et al. The Possible Side Reaction in the Annealing Process of Perovskite Layers. ACS Appl Mater Interfaces. 2020 Aug 5;12(31):35043–8.

10. Song Z, Wang C, B. Phillips A, R. Grice C, Zhao D, Yu Y, et al. Probing the origins of photodegradation in organic–inorganic metal halide perovskites with time-resolved mass spectrometry. Sustain Energy Fuels. 2018;2(11):2460–7.

11. Valenzano V, Cesari A, Balzano F, Milella A, Fracassi F, Listorti A, et al. Methylammonium-formamidinium reactivity in aged organometal halide perovskite inks. Cell Rep Phys Sci. 2021 May 19;2(5):100432.

12. Wang M, Shi Z, Fei C, Deng ZJD, Yang G, Dunfield SP, et al. Ammonium cations with high pKa in perovskite solar cells for improved high-temperature photostability. Nat Energy. 2023 Nov;8(11):1229–39.

13. Chen B, Chen H, Hou Y, Xu J, Teale S, Bertens K, et al. Passivation of the Buried Interface via Preferential Crystallization of 2D Perovskite on Metal Oxide Transport Layers. Adv Mater. 2021;33(41):2103394.

14. Kubicki DJ, Prochowicz D, Hofstetter A, Saski M, Yadav P, Bi D, et al. Formation of Stable Mixed Guanidinium–Methylammonium Phases with Exceptionally Long Carrier Lifetimes for High-Efficiency Lead Iodide-Based Perovskite Photovoltaics. J Am Chem Soc. 2018 Mar 7;140(9):3345–51.

15. De Marco N, Zhou H, Chen Q, Sun P, Liu Z, Meng L, et al. Guanidinium: A Route to Enhanced Carrier Lifetime and Open-Circuit Voltage in Hybrid Perovskite Solar Cells. Nano Lett. 2016 Feb 10;16(2):1009–16.

16. Jiang Q, Tong J, Xian Y, Kerner RA, Dunfield SP, Xiao C, et al. Surface reaction for efficient and stable inverted perovskite solar cells. Nature. 2022 Nov;611(7935):278–83.

17. Zhang F, Cong J, Li Y, Bergstrand J, Liu H, Cai B, et al. A facile route to grain morphology controllable perovskite thin films towards highly efficient perovskite solar cells. Nano Energy. 2018 Nov 1;53:405–14.

18. Mateen M, Arain Z, Liu X, Iqbal A, Ren Y, Zhang X, et al. Boosting optoelectronic performance of MAPbI3 perovskite solar cells via ethylammonium chloride additive engineering. Sci China Mater. 2020 Dec 1;63(12):2477–86.

19. Xu S, Ding X, Shi H, Zhang X, Sun X, Ji N, et al. EA-Directing Formamidinium-Based Perovskite Microwires with A-Site Doping. ACS Omega. 2021 Mar 16;6(10):7157–64.

20. Tsiba Matondo J, Zhang Y, Yang Y, Mbumba MT, Akram MW, Malouangou MD, et al. Effect of Organic Chloride Additives on the Photovoltaic Performance of MA-Free Cs0.1FA0.9PbI3 Perovskite Solar Cells. Sol RRL. 2023;7(4):2200950.

21. Nishi K, Oku T, Kishimoto T, Ueoka N, Suzuki A. Photovoltaic Characteristics of CH3NH3PbI3 Perovskite Solar Cells Added with Ethylammonium Bromide and Formamidinium Iodide. Coatings. 2020 Apr;10(4):410.

22. Huang Y, Jiang Y, Zou S, Zhang Z, Jin J, He R, et al. Substitution of Ethylammonium Halides Enabling Lead-Free Tin-Based Perovskite Solar Cells with Enhanced Efficiency and Stability. ACS Appl Mater Interfaces. 2023 Mar 29;15(12):15775–84.

23. Zhang Y, Park NG. A thin film (<200 nm) perovskite solar cell with 18% efficiency. J Mater Chem A. 2020 Sep 1;8(34):17420–8.

24. Zhang Y, Kim SG, Lee D, Shin H, Park NG. Bifacial stamping for high efficiency perovskite solar cells. Energy Environ Sci. 2019 Jan 16;12(1):308–21.

25. Park B wook, Kwon HW, Lee Y, Lee DY, Kim MG, Kim G, et al. Stabilization of formamidinium lead triiodide α-phase with isopropylammonium chloride for perovskite solar cells. Nat Energy. 2021 Apr;6(4):419–28.

26. Kim H, Lee S, Lee DY, Paik MJ, Na H, Lee J, et al. Optimal Interfacial Engineering with Different Length of Alkylammonium Halide for Efficient and Stable Perovskite Solar Cells. Adv Energy Mater. 2019 Dec;9(47):1902740.

27. Jariwala S, Burke S, Dunfield S, Shallcross RC, Taddei M, Wang J, et al. Reducing Surface Recombination Velocity of Methylammonium-Free Mixed-Cation Mixed-Halide Perovskites via Surface Passivation. Chem Mater. 2021 Jul 13;33(13):5035–44.

28. Stolterfoht M, Grischek M, Caprioglio P, Wolff CM, Gutierrez-Partida E, Peña-Camargo F, et al. How To Quantify the Efficiency Potential of Neat Perovskite Films: Perovskite Semiconductors with an Implied Efficiency Exceeding 28%. Adv Mater. 2020;32(17):2000080.

29. de Mello JC, Wittmann HF, Friend RH. An improved experimental determination of external photoluminescence quantum efficiency. Adv Mater. 1997;9(3):230–2.

30. Liu D, Li Q, Wu K. Ethylammonium as an alternative cation for efficient perovskite solar cells from first-principles calculations. RSC Adv. 2019 Mar 1;9(13):7356–61.

31. Shi P, Ding Y, Ding B, Xing Q, Kodalle T, Sutter-Fella CM, et al. Oriented nucleation in formamidinium perovskite for photovoltaics. Nature. 2023 Aug;620(7973):323–7.

32. Al-Ashouri A, Magomedov A, Roß M, Jošt M, Talaikis M, Chistiakova G, et al. Conformal monolayer contacts with lossless interfaces for perovskite single junction and

monolithic tandem solar cells. Energy Environ Sci. 2019 Nov 6;12(11):3356–69.

33. Weber OJ, Ghosh D, Gaines S, Henry PF, Walker AB, Islam MS, et al. Phase Behavior and Polymorphism of Formamidinium Lead Iodide. Chem Mater. 2018 Jun 12;30(11):3768–78.

The data supporting this article have been included as part of the Supplementary Information.